THE AMERICAN MINERALOGIST, VOL. 50, NOVEMBER–DECEMBER, 1965

PROTON DELOCALIZATION IN MICAS

J. J. Fripiat,[1] P. Rouxhet[2] and H. Jacobs

Laboratoire de physico-chimie minérale, Agronomic Institute of the University of Louvain, Héverlé-Louvain, Belgium.

Abstract

The infrared absorption bands due to OH fundamental stretching vibrations of micas have been studied at increasing temperature. To interpret the decreasing intensity of these bands with increasing temperature, it is suggested that dehydroxylation is preceded by a reversible process described as a delocalization of constitutional protons. Attention is given to a possible modification of the OH ion orientation upon heating but this fails apparently to explain the loss in intensity. A qualitative wave-mechanical model is tentatively proposed to depict the proton delocalization. In the appendix, a statistical thermodynamics treatment is developed which aims to correlate thermal stability with octahedral composition.

Introduction

Dehydroxylation of minerals is probably preceded by an increase in the mobility of constitutional protons. The change in the infrared OH stretching vibration bands of crystals heated to progressively higher temperatures has been used for studying dehydroxylation of kaolinite. For this mineral, Fripiat and Toussaint (1963) have defined a "pre-dehydroxylation state" characterized by the delocalization of constitutional protons within the octahedral layers. The crystal has to be brought to this state before the weight loss becomes noticeable.

Thin mica flakes are convenient materials with which to work and infrared investigations by Tsuboi (1950), by Serratosa and Bradley (1958), and by Vedder and McDonald (1963) have given interesting information on the hydroxylic structure at room temperature. More recently, Vedder (1964) showed correlations between the infrared spectra and chemical compositions of muscovite and phlogopite; moreover, for phlogopite especially, the intensity of the fundamental stretching frequency rapidly decreases with increasing temperature.

The aim of this investigation is to study the OH behavior before dehydroxylation by an analysis of the infrared stretching vibration bands of micas at increasing temperatures.

Experimental

Materials. The samples were chosen in order to cover a large variety of compositions and infrared spectral types as shown in Fig. 1. Muscovite was from Rivière Grande (Kamituga, Congo Rep.). Two biotite samples

[1] M.R.A.C. (Tervuren) and the University of Louvain.

[2] On leave of absence from the "Laboratoire de physicochimie minérale, Louvain" at Materials Research Laboratory, The Pennsylvania State University, University Park (Pa.)

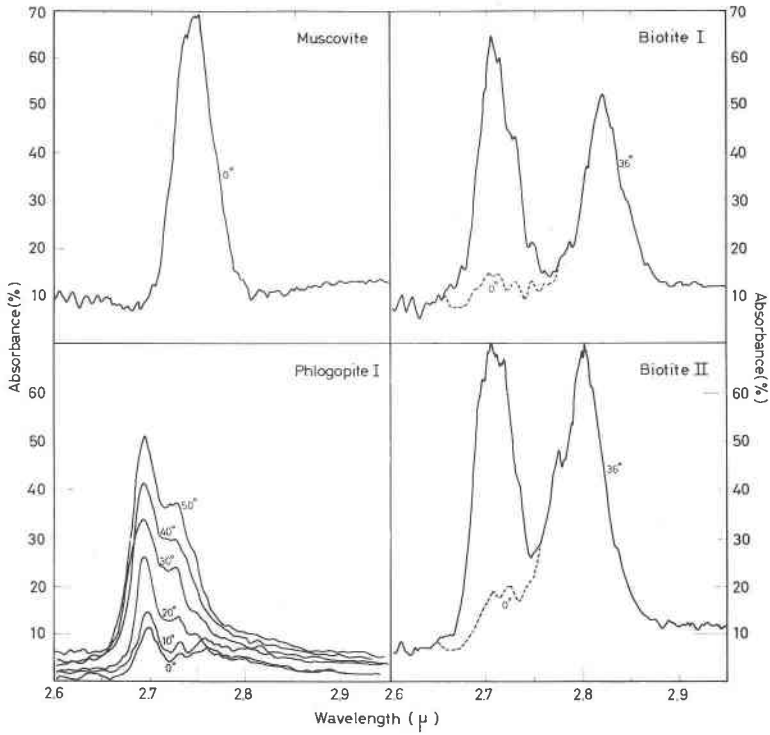

FIG. 1. Some examples of infrared spectra at room temperature. Muscovite (normal incidence). Biotite I and Biotite II, tilted at 36° in the beam. Phlogopite I at different incidence angles.

were studied: the first from Luindi (Congo Rep.) and the second from Bancroft (Ontario, Canada). Phlogopite I was from Odegarden (Norway) and phlogopite II from Madagascar. The structural formulae calculated according to the chemical analysis are indicated in Table 1. Mica flakes were obtained by cleaving the minerals and were selected for uniform thickness.

Apparatus. The infrared spectrophotometer was the Beckman IR4 fitted with CaF_2 optics. It was operated at low scanning speed (0.1 or 0.04μ min^{-1}). The infrared cell permits 1) the c^* axis of the crystal to be tilted in the beam by rotating the flake around the a or b axis, and 2) the sample to be heated up to 900° C. in an iner atmosphere (N_2) to prevent oxidation of Iron II.

The absorbance spectra were recorded between 3 and 2.5μ and the peak heights measured above the background line. In the case of musco-

TABLE 1. STRUCTURAL FORMULAE OF MICAS

	Muscovite	Biotite I	Biotite II	Phlogopite I	Phlogopite II
Tetrahedral layer					
Si^{4+}	3.09	2.875	2.99	2.866	2.76
Al^{3+}	0.91	1.125	1.01	1.134	1.24
Octahedral layer					
Al^{3+}	1.755	—	—	0.24	0.077
Fe^{3+}	0.101	0.265	0.150	0.018	0.097
Mg^{2+}	0.149	0.995	1.540	2.354	2.430
Fe^{2+}	0.036	1.318	1.013	0.206	0.174
Ti^{4}	0.008	0.191	0.129	0.154	0.059
Li^{+}	—	0.014	0.079	—	—
Cations					
Na^{+}	0.093	0.033	0.066	0.202	0.114
K^{+}	0.824	0.849	0.864	0.711	0.858
Ca^{2+}	0.007	0.007	—	—	—
Octahedral population per three sites	2.049	2.783	2.911	2.972	2.837

Analyses by L. Vielvoye, Analytical service of the laboratory.

vite where a single OH band is observed, the intensity has been calculated by integrating the absorbance against the wavelength. For biotite, the peak height was chosen as a measurement of the absorbance since the overlapping of the two bands precludes the integration of each of them. For phlogopite, integration and peak height measurement were used indiscriminately.

Since the light is chopped when entering and leaving the cell, the infrared thermal emission of the hot cell does not noticeably affect the beam. To check this, a thoroughly dehydroxylated specimen was introduced in the cell and heated at the same temperature as that for the studied sample and no emission or absorption could be recorded.

ABSORPTION COEFFICIENT MEASUREMENTS

The muscovite spectrum shows only weak intensity changes on tilting the flake in the beam (Fig. 1). On the contrary, the fundamental OH band of phlogopite is very weak at normal incidence and grows more intense when tilted, as shown in Fig. 1. In biotite, the intensity of the low frequency OH fundamental does not depend on the orientation while the high frequency fundamental reacts in the same way as the phlogopite

band. These basic differences originate from the orientation of the OH ions, as pointed out by Serratosa and Bradley (1958a).

This orientation can be explained if the OH bond is related to oxygen orbitals (*cf.* Serratosa and Bradley, 1958b). In dioctahedral structures the oxygen atom of the hydroxyl group has two orbitals which are available for the proton; the orbital tilted on the 001 plane seems to be the preferred one. When the octahedral hole is occupied by a metal cation, as in trioctahedral structures, the proton has to take the second orbital which is almost perpendicular to the (001) plane.

The correlation between the band intensities and the absorption coefficients results from the following consideration. Let the polarized infrared radiation pass through an absorbing material in which the oscillating dipoles have a fixed direction. The Beer-Lambert law appears as follows:

$$I/I_0 = \exp(-ke\cos^2\chi/\cos r)$$

where r is the refraction angle, χ the angle between the electrical field vector of the beam and the vibrational moment, e the thickness of the crystal, and k the absorption coefficient of a system where the directions of the resonating electrical vectors would be parallel.

In addition, account must be taken of the light polarization by the mineral. Let a and b represent the intersections of the polarization planes of the mineral with the plane scanned by the electrical field vector $\vec{V}$. If the beam is perpendicular to the flake, a and b correspond with the lattice axes. The two components I_{0_a} and I_{0_b} of $\vec{V}$ along a and b are:

$$I_{0_a} = I_0\cos^2\theta \quad \text{and} \quad I_{0_b} = I_0\sin^2\theta \tag{2}$$

where θ is the angle between $\vec{V}$ and a. The corresponding intensities emerging from the crystal being I_a and I_b, the transmissions of the radiation polarized along a and b, are:

$$m_a = \frac{I_a}{I_0\cos^2\theta} \quad \text{and} \quad m_b = \frac{I_b}{I_0\sin^2\theta} \tag{3}$$

respectively and, in accordance with Tsuboi (1950), the resulting transmission is $m = m_a\cos^2\theta + m_b\sin^2\theta$. For an unpolarized incident beam, all the θ angles between 0 and 2π are scanned by $\vec{V}$ and the average value of m is $\bar{m} = \frac{1}{2}(m_a + m_b)$.

The absorbance $A = \log I_0/I$ is given by:

$$A = \log 2 - \log\left[e^{-ke\cos^2\alpha/\cos r} + e^{-ke\cos^2\beta/\cos r}\right] \tag{4}$$

where α and β are the angles between the vibrational moments and the components of the electrical field vector polarized in the ac* and bc* planes of the lattice. The polarization ellipsoid is almost spherical so that only a single diffraction angle has to be considered.

Muscovite. Figure 2 (A and B) represents, according to Vedder and McDonald (1963), the directions of vibrational moments d with respect to the lattice axes. These moments are tilted away from the cleavage plane by about $\pm 16°$ and their projections onto the cleavage plane make an

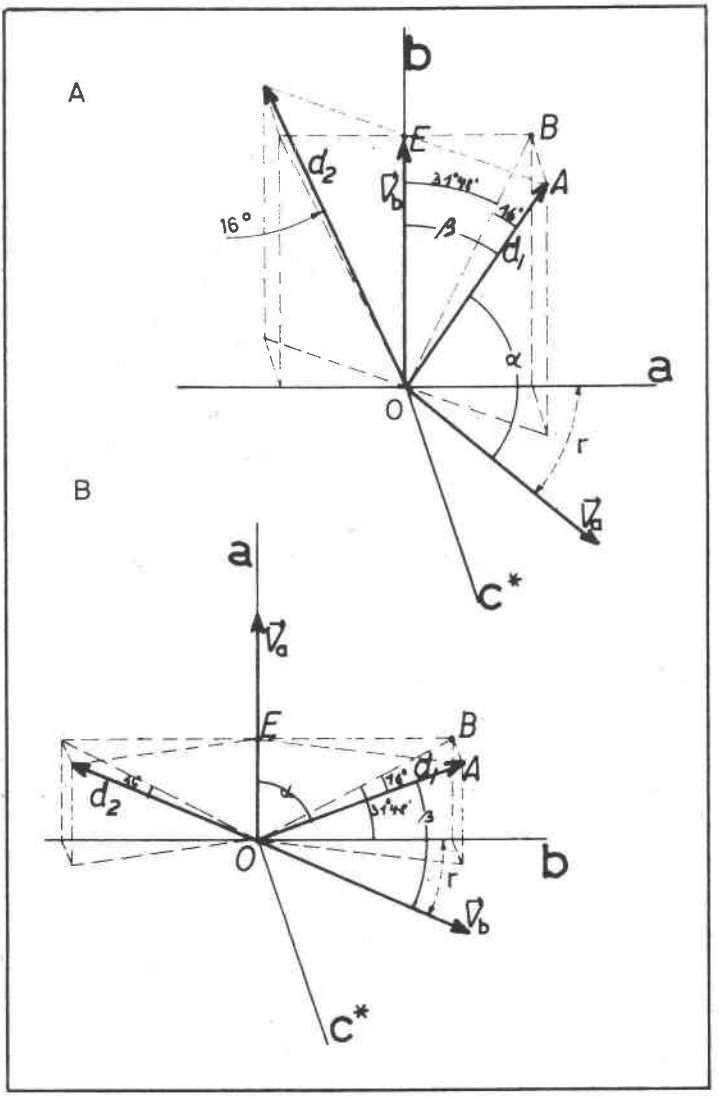

FIG. 2. Directions of OH vibrational moments (d_1 and d_2) in muscovite according to Vedder and McDonald. A) Rotation of the flake around the *b* axis; B) rotation around the *a* axis.

angle of about $\pm 32°$ with the *b* axis. This azimuthal angle should be of 30° in an ideal lattice without distortion. The vibrational directions are approximately those of OH dipoles, the restriction being due to the value of the unknown moment induced by the crystal field. The direction of

the electrical field components $\vec{V}_a$ and $\vec{V}_b$ results from the coincidence of the crystal axes a, b and c^* with the axes of the polarization ellipsoid for the monoclinic system.

Let us assume that the beam direction in the crystal is perpendicular to the b axis and, for a rotation about this axis, makes an angle r with the a axis (Fig. 2A). The angle between $\vec{V}_a$ (polarized in the ac* plane) and a is r; $\vec{V}_b$ coincides with b for any r. The symmetrical situation for a rotation around the a axis is shown in Fig. 2B. From these models $\cos^2 \alpha$ and $\cos^2 \beta$ of relation (4) may be easily calculated:

Beam perpendicular to b or rotation around b

$$\cos^2 \beta = 0.667$$
$$\cos^2 \alpha = (0.506 \cos r + 0.275 \sin r)^2 \quad (5)$$

Beam perpendicular to a or rotation around a

$$\cos^2 \alpha = 0.256$$
$$\cos^2 \beta = 0.075 \sin^2 r + 0.667 \cos^2 r \quad (6)$$

The refractive index of muscovite has been taken equal to 1.615 (Vedder and McDonald, 1963). As shown in Fig. 3A, the experimental data agree well with relationship (4), in which the corresponding $\cos^2 \alpha$ and $\cos^2 \beta$ values for both situations have been introduced. The ke values have been obtained from measurements performed on flakes normal to the beam.

Interpretation of the OH bond directions in terms of orbitals agrees perfectly with these angle values if one considers the polymorphic structure of muscovite and the symmetry of the octahedral hole. Natural muscovite is $2M_1$ according to Smith and Yoder (1956). Depending on the distribution of the octahedral cations around the octahedral hole, its symmetry may be 2 or $2/m$. Figure 4 shows that this symmetry group has to determine the OH directions with respect to the t translation vector. If it is assumed that the 16° angle with the (001) plane is not changed and if the lattice distortions pointed out by Radoslovich (1960), Vedder (1964) and others are neglected, Fig. 5A can be drawn. It shows that the OH model of muscovite corresponds actually to the $2M_1$ polymorphic structure and $2/m$ octahedral hole symmetry. Therefore the localization of the OH bond inside the mica layer by orbital directions has to be accepted.

Biotite. The intensity of the *low frequency* (*LF*) *band* of biotite (a muscovite-like band) does not depend on the orientation of the crystal around a or b. Since the free octahedral positions in biotite are probably randomly distributed, the statistical weight of the octahedral holes belonging to the symmetry group 2 is double that for those belonging to the

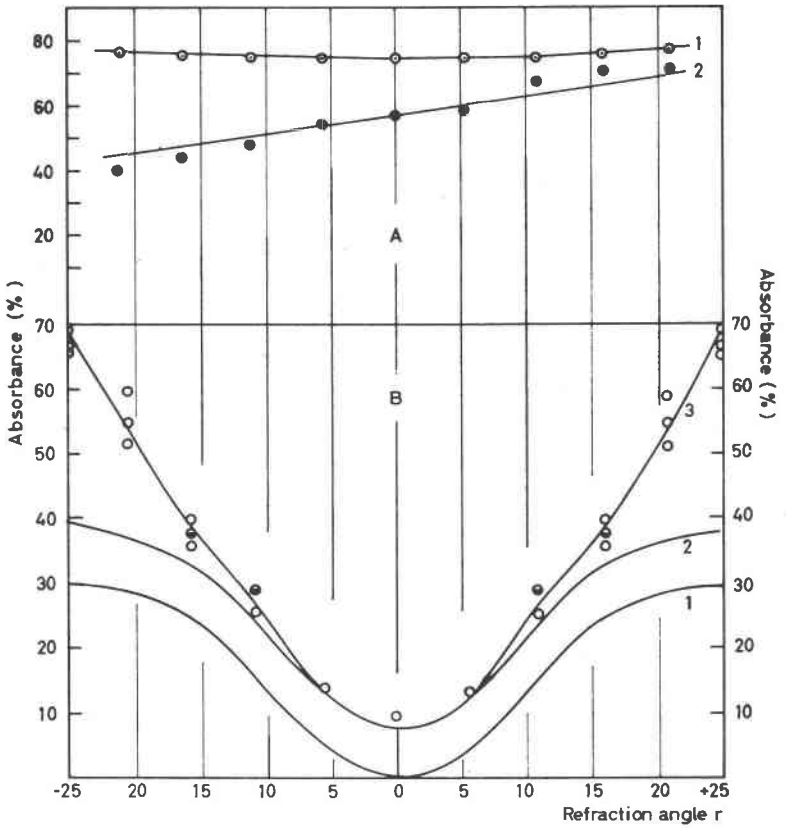

FIG. 3. A. Absorbance against refraction angle r for two different muscovite flakes rotated around the a axis ○ and the b axis ●. Solid lines: theoretical functions calculated according to relationships (4) and (6) for 1, (4) and (5) for 2. B. Absorbance of the high frequency band of biotites against refraction angle r. 1, theoretical function calculated according to (8); 2, theoretical function calculated according to (11), $\gamma = 7°$, reflections neglected; 3, as curve 2 but taking into account nine reflections. Experimental points: O: Biotite II, ◒: Biotite I.

symmetry group $2/m$. The superposition of the structures, shown in Fig. 5A, by taking account of their statistical weights, leads to the models represented in Fig. 5B. A single relationship between A and r is then obtained for these different polymorphic structures oriented around the a and b axes.

$$A = \log 2 - \log \left[\exp \left(- \frac{ke}{\cos r} 1/2 \cos^2 16° \right) + \exp \left\{ - \frac{ke}{\cos r} (\sin^2 16° \sin^2 r + 1/2 \cos^2 r \cos^2 16°) \right\} \right] \quad (7)$$

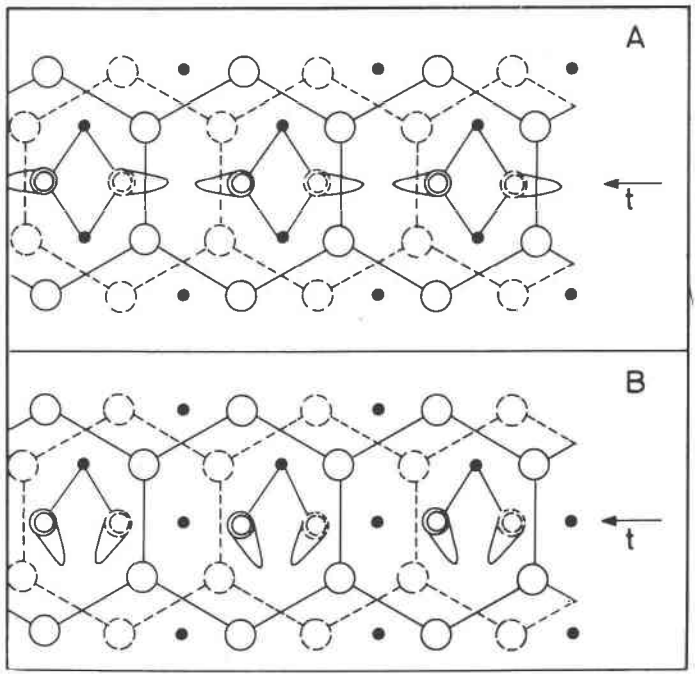

FIG. 4. Projection of the octahedral layer on the (001) plane. A: $2/m$ symmetry. B: 2 symmetry. ○: Oxygen atom of the upper plane; ◌: Oxygen atom of the lower plane; ◎: Hydroxyl oxygen atom of the upper plane; ⊛: Hydroxyl oxygen atom of the lower plane; half ellipses represent O-H bonds; t: translation vector; ●: Cation of the octahedral layer.

The refractive index used for biotite is 1.66 which is close to a value measured with visible light. Such an approximation, does not affect seriously the final results as shown by Tsuboi (1950). The calculations carried out according to relation (7) show that A is constant regardless of the angle r; this has been checked experimentally within $\pm 2\%$ absorbance.

The *high frequency (HF) band* observed in biotite is strongly dependent on the orientation; it corresponds to vibrational moments oriented almost perpendicularly to the cleavage plane towards the hexagonal hole of the basal planes. For perpendicular orientation:

$$A = \log 2 - \log (1 + e^{-ke \sin^2 r/\cos r}) \qquad (8)$$

From relationship (8), the absorbance should never be higher than 30%, which is in contradiction with the experimental data. This discrepancy arises from the energy loss resulting from reflections undergone by the

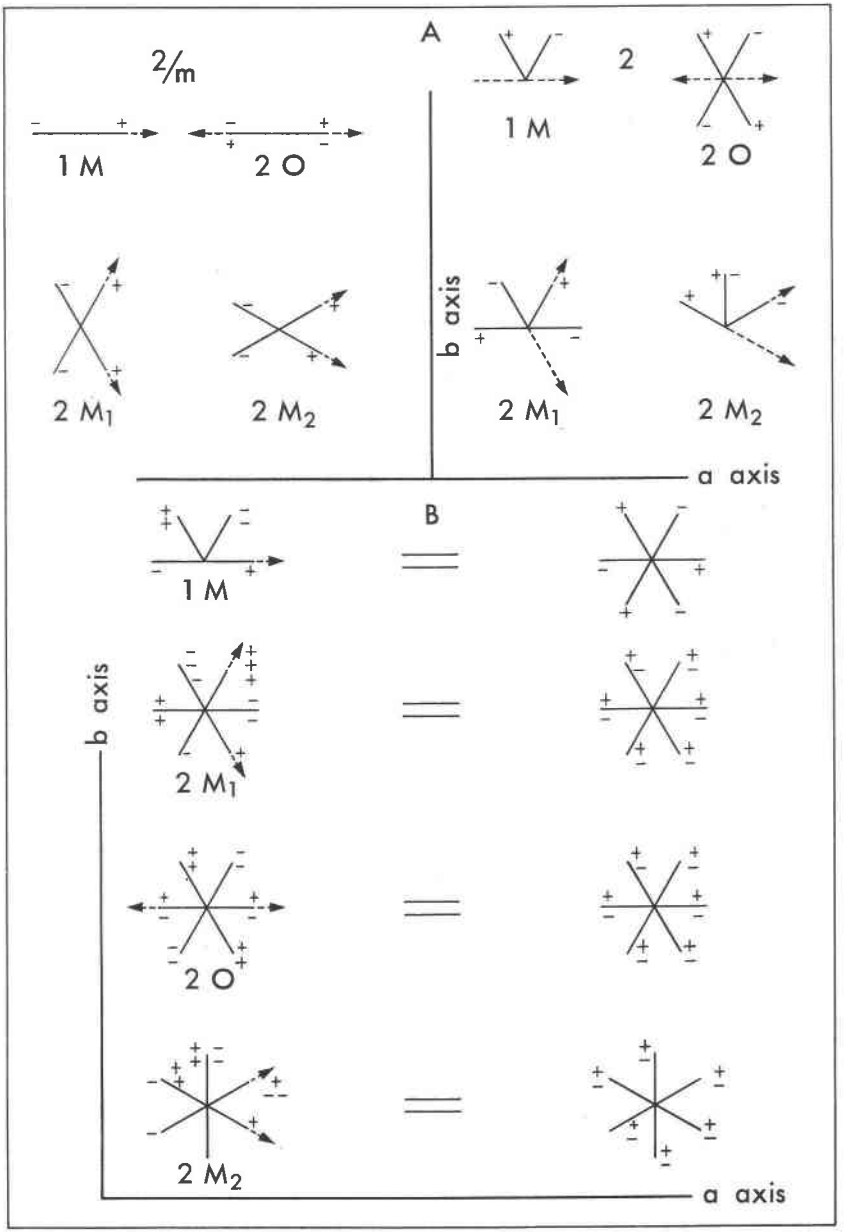

FIG. 5. Polymorphic structures of micas: A. Projection of the OH ion direction on (001) plane: OH tilted 16° away above (— +) and under (— —) this plane, translation vector t(-→). B. Combinations of the symmetry groups $2/m$ and 2 in the proportion two (2) to one ($2/m$).

radiation at lamellar surface. For the thin and very coherent flakes of muscovite two reflections on the limiting planes did not perturb noticeably the transmission. For the thicker and less coherent flakes of biotite, corrections founded on Fresnel relationships (9) must be used. The energy contributions of the polarized beams to the transmitted radiation after N reflections are defined by

$$F_{\perp} = \frac{2(1-\varphi_{\perp})^N}{(1-\varphi_{\perp})^N + (1-\varphi_{\parallel})^N}$$

and

$$F_{\parallel} = \frac{2(1-\varphi_{\parallel})^N}{(1-\varphi_{\perp})^N + (1-\varphi_{\parallel})^N} = 2 - F_{\perp}$$

where

$$\frac{I_{refl.}}{I_{incid.}} = \left(\frac{\sin(r-i)}{\sin(r+i)}\right)^2 = \varphi_{\perp} \quad \text{for the electrical vector perpendicular to the incidence plane}$$

$$\frac{I_{refl.}}{I_{incid.}} = \left(\frac{\tan(r-i)}{\tan(r+i)}\right)^2 = \varphi_{\parallel} \quad \text{for the electrical vector parallel to the incidence plane} \qquad (9)$$

r and i represent the refraction and incidence angles respectively.

The absorbance of the HF band is then as follows:

$$A = \log 2 - \log\left[F_{\perp} + F_{\parallel} \exp\left(-ke \sin^2 r/\cos r\right)\right] \qquad (10)$$

It is unnecessary to take account of the reflections for the LF band because the two exponential terms are almost equal in (7); the influence of reflections is therefore very small.

Figure 3B shows observed and theoretical absorbances, derived from relation (10) for the high frequency band. Since the absorbance for $r=0°$ is not zero, a small deviation of the vibrational moment from the normal has to be considered. By assuming that the deviation angle γ away from the normal to the cleavage plane is constant and that the distribution of azimuths has at least a three-fold symmetry, a relationship similar to (7) but corrected for surface reflections is obtained:

$$A = \log 2 - \log\left[F_{\perp} \exp\left\{-\frac{ke}{\cos r} 1/2 \cos^2\left(\frac{\pi}{2}-\gamma\right)\right\} + F_{\parallel} \exp\left\{-\frac{ke}{\cos r}\left(\sin^2 r \sin^2\left(\frac{\pi}{2}-\gamma\right) + 1/2 \cos^2 r \cos^2\left(\frac{\pi}{2}-\gamma\right)\right)\right\}\right] \qquad (11)$$

This expression is applicable for rotation around both a and b axes. Figure 3B shows that the best fit between theoretical and experimental data is obtained for $\gamma = 7°$ and for approximately nine reflections.

Phlogopite. In this case, the situation is similar to that for the high fre-

quency band of biotite and relationship (11) has to be applied. A refractive index measured in visible light (1.58) was again extrapolated for the calculation of r. Figure 6 shows experimental and theoretical absorbance variations with respect to r for $\gamma = 7°$.

For phlogopite, it is interesting to point out that the force field model proposed by Vedder (1964) in order to explain the orientation of OH ions predicts a deviation of the OH orientation from the perpendicular in the order of 0–15° possibly with considerable preference for angles of about 8°.

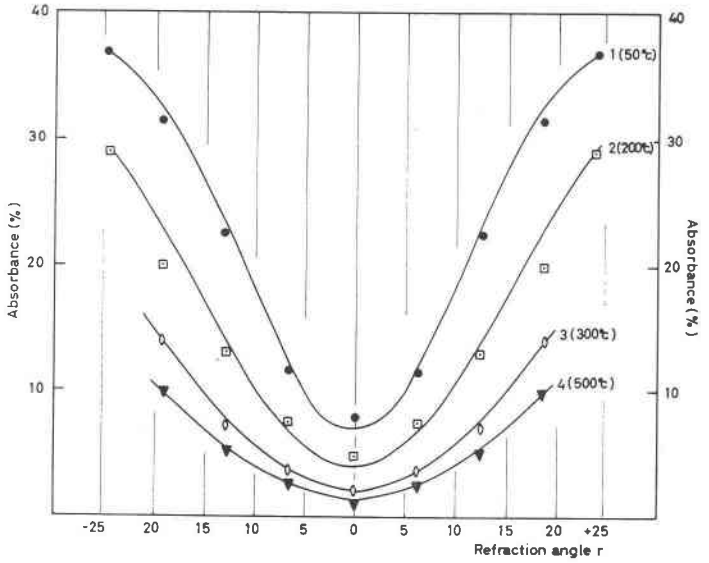

FIG. 6. Phlogopite II. Absorbance against refraction angle r. Solid line: theoretical function calculated according to (11): $\gamma = 7°$, no reflection. 1: ke=21; 2: ke=11.9; 3: ke=5.7; 4: ke=4.2. The corresponding temperatures are indicated.

In summary, from relationships (4), (5) and (6) for muscovite and (7) and (11) for biotite (LF and HF bands respectively), and (11) for phlogopite, the *ke* values were calculated for the best agreement between experimental and theoretical data.

RESULTS

The OH fundamental band of muscovite is almost symmetrical and centered on 3640 cm^{-1} at 30° C. The frequency decreases almost linearly to 3620 cm^{-1} on increasing the temperature to 700° C. (Fig. 7). The high frequency bands, which are very sensitive to the orientation, are ob-

served at 3690 cm^{-1} and at 3696 cm^{-1} for biotites I and II respectively. The low frequency bands appear at 3571 cm^{-1} and 3543 cm^{-1} correspondingly. The frequency of the HF band seems approximately independent of temperature while the LF band shifts slightly towards higher frequencies upon heating. In phlogopite I, the OH fundamental is observed at 3718 cm^{-1} at 50° C. and its frequency decreases linearly to 3698 cm^{-1} at 600° C. (Fig. 7).

The OH · · · O bond length modifications corresponding with these

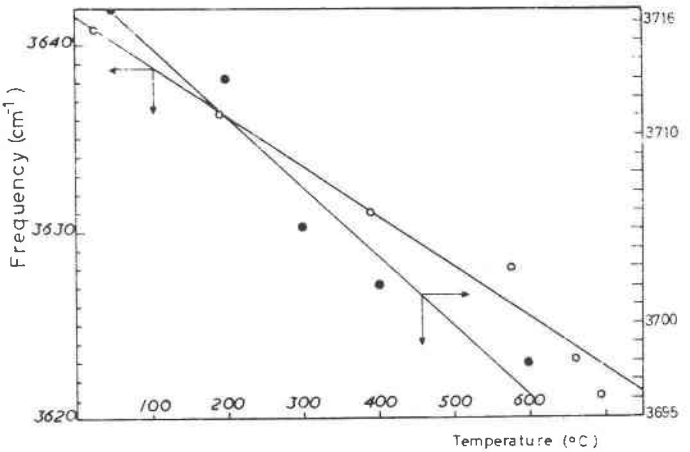

FIG. 7. Frequency shifts of fundamental ν_{OH} against temperature. ○, Muscovite; ●, Phlogopite I. The scales corresponding to each straight line are indicated by arrows.

small thermal shifts do not suggest an appreciable perturbation in the orientation of the vibrational moments.

However, the intensity loss of the OH fundamental stretching bands upon heating is extremely important; it is conveniently expressed by the variation of $\alpha = ke/(ke)_0$ with respect to the temperature as shown in Fig. 8. The HF band of the biotites did not allow quantitative measurements to be made. It should be emphasized that the initial $(ke)_0$ values obtained at 30° C. are restored after cooling muscovite heated to 600° C. for 20 minutes. Under the same conditions, this reversibility is also observed for phlogopite heated to 500° C. and for biotite heated to 400° C. When samples treated at higher temperatures or for longer times are cooled to 30° C., the measured values of $(ke)_0$ are lower than the initial ones as a result of partial dehydroxylation, but the relative $ke/(ke)_0$ calculated for a second heating cycle and plotted against T fit the function measured for the first cycle. For measurements under conditions where dehydroxylation occurred, the sample was cooled as quickly as possible after recording

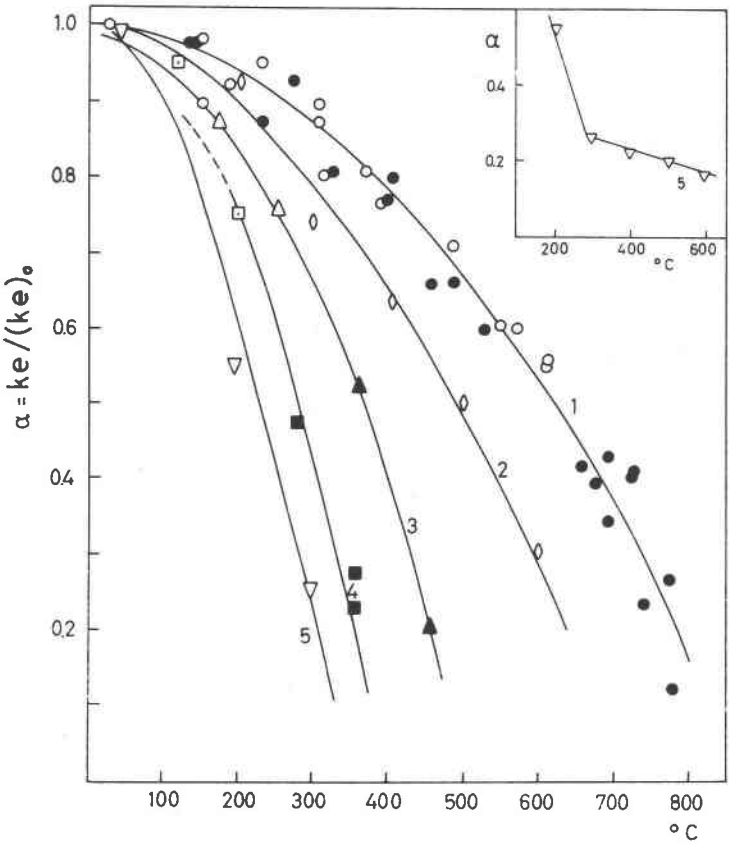

FIG. 8. $\alpha = ke/(ke)_0$ against temperature (°C). 1, Muscovite. 2, Phlogopite I. 3, Biotite II (LF). 4, Biotite I (LF). 5, Phlogopite II. White symbols: α calculated from the initial value of $(ke)_0$. Black symbols: samples partially dehydroxylated.

the spectrum and the corresponding $(ke)_0$ value was calculated from a new spectrum at room temperature. The intensity loss appears, therefore, as a reversible process which should be explained by 1) reversible changes in the orientations of vibrational moments, 2) a reversible delocalization process which moves the constitutional protons towards interstitial positions or vacancies of the crystal lattice.

Noticeable changes in the orientations of vibrational moments seem to be ruled out by the following considerations. The absorbances of muscovite flakes at a rather high temperature, corresponding to $ke/(ke)_0 = 0.5$, have been tentatively calculated by lowering ke to $(ke)_0/2$ but keeping $\cos\alpha$ and $\cos\beta$ constant, or by keeping $ke = (ke)_0$ and changing $\cos\alpha$ and $\cos\beta$. In the second case, the calculations were carried out by increasing

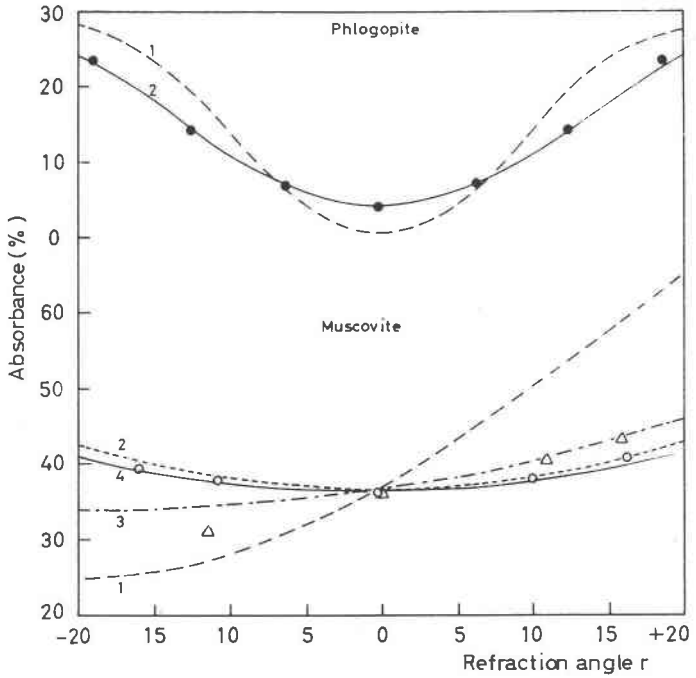

FIG. 9. *Phlogopite I;* Dashed line: Theoretical function calculated from relationship (8), $\gamma = 0°$ and ke = 23. Solid line: theoretical function calculated from relationship (11), $\gamma = 7°$ and ke = 11.5. ●: experimental absorbance at 500° C.

Muscovite: 1 and 2: theoretical functions calculated for rotation around the *b* and *a* axes respectively; ke = 4; vibrational moment tilted at 46°41′ on the cleavage plane. 3 and 4: theoretical functions calculated for rotation around the *b* and *a* axes respectively; ke = 2, vibrational moment tilted at 16° on the cleavage plane. ○ : absorbances observed for a rotation around *a*; △: absorbances observed for a rotation around *b*, both at 600° C.

the tilt of the vibrational moment on the cleavage plane, the azimuth of 30–32° being unchanged.[1] Results are shown in Fig. 9. For muscovite, the intensity loss requires the tilt to increase from 16° to 46°41′ but under these conditions rotation around the *b* axis gives a theoretical function which obviously does not fit the experimental points. On the contrary, lowering ke to $\frac{1}{2}(ke)_0$ restores a much better fit. Rotation around the *a* axis does not distinguish between delocalization or orientation change. For phlogopite the uncertainty in the peak intensities at normal incidence requires the calculation to be based on some angle other than $r = 0$. By keeping $ke = (ke)_0$, the observed absorbance value at $r = 7°$ is re-

[1] Constancy of the azimuth angle 30–32° has been proved by using a polarized infrared beam. See "Note sur la constance de l'orientation du vibrateur OH dans la muscovite chauffée": to be published in *Silicates Industriels*, 1966.

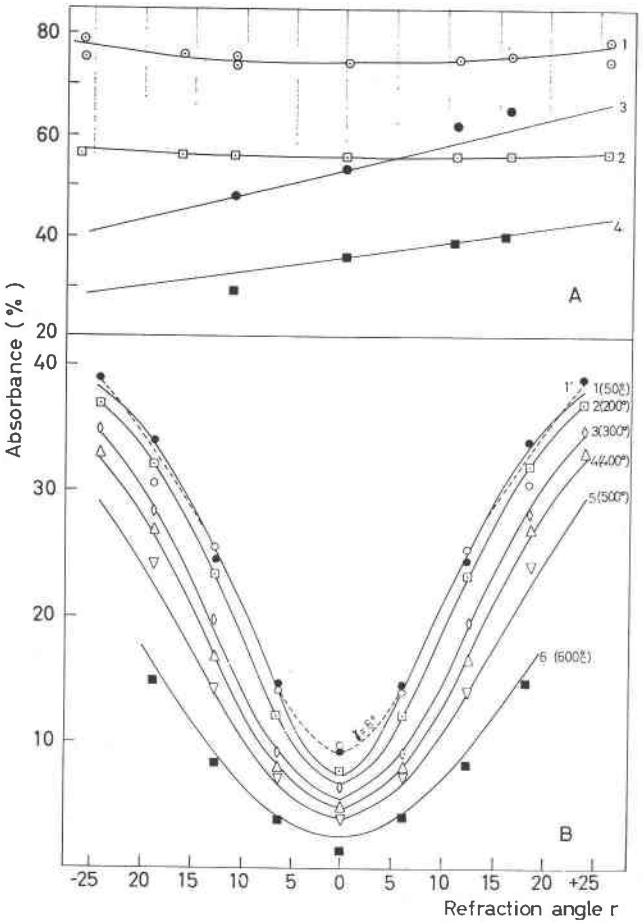

FIG. 10. Constancy of orientations of vibrational moments in a broad temperature range. Solid lines: theoretical functions.

A. Muscovite: 1, rotation around the *a* axis; ○ absorbances observed for a sample cooled at 30° C. after having been heated at 490° C. and 515° C. 2, rotation around the *a* axis; □: sample at 490° C. 3, rotation around the *b* axis; ●: sample cooled at 30° C. after treatment at 695° C. 4, rotation around the *b* axis; ■: sample at 615° C.

B. Phlogopite I, $\gamma = 7°$, ke equal respectively to: 1: 23; 2: 21.1; 3: 17.2; 4: 14.6; 5: 11.5; 6: 7.0. Experimental results represented for the flake heated at the following temperatures: 1: 50° C.; 2: 200° C.; 3: 300° C.; 4: 400° C.; 5: 500° C.; 6: 600° C.

stored by diminishing γ to zero but then the angular variation does not fit the experimental points.

Figures 6 and 10 supply additional confirmations of the approximate constancy of the orientations of vibrational moments.

The conclusion, therefore, is that the intensity of the OH fundamental stretching bands is a function of the degree of delocalization of constitu-

tional protons. The slope of the variation of $ke/(ke)_0$ against the temperature decreases to zero as room temperature is approached (Fig. 8). and consequently, it will be assumed that at 30° C. protons are not delocalized to an appreciable extent.

Discussion

If the proton delocalization is considered as a chemical reaction, it may be represented by the following equation: $-OH+$interstitial sites$\rightleftharpoons H^+$ moving on interstitial positions$+-O^-$. Let N_{OH} be the number of hydroxyls, N_i the number of interstitial sites and n_i the number of interstitial protons per unit volume; the equilibrium constant may be written as:

$$K = \frac{n_i^2}{N_{OH}N_i} = \frac{N_{OH}^0(1-\alpha)^2}{N_i\alpha} \tag{12}$$

where $\alpha = ke/(ke)_0$ and N_{OH}^0 is the number of hydroxyls per unit volume under temperature conditions such that delocalization is negligible. If N_i can be considered to be constant,

$$K = c\frac{(1-\alpha)^2}{\alpha}$$

where $c = N_{OH}^0/N_i$.

Figure 8 shows that delocalization is, to some extent, independent of the degree of dehydroxylation but the shape of the function $\alpha(T)$ must change above the dehydroxylation temperature. This has been checked experimentally for Phlogopite II; *ke* measurements were made at high temperature, immediately preceded and followed by $(ke)_0$ determinations on samples cooled very rapidly and the average $(ke)_0$ was used for determining α. The insert in Fig. 8 shows the results. Therefore it is meaningless to extrapolate $\alpha(T)$ functions to $\alpha=0$ and to characterize each mica by a temperature at which delocalization should be apparently complete. That the α values for muscovite, measured for partially dehydroxylated minerals, fit the function obtained for intact material is probably because water nucleation occurs in large crystals or in complete octahedral layers of a crystal at once (Fripiat and Toussaint, 1963). Although consideration of delocalization as a reversible equilibrium process leads to interesting deductions, they are founded on hypotheses, so that the thermodynamic treatment of these data will be given in the appendix.

More simply, delocalization may be considered as a transition of the proton to an excited state: the Boltzmann relation may then be applied as follows:

$$1 - \alpha = B \exp(-E/RT) \tag{13}$$

where E is the activation energy for the delocalization.

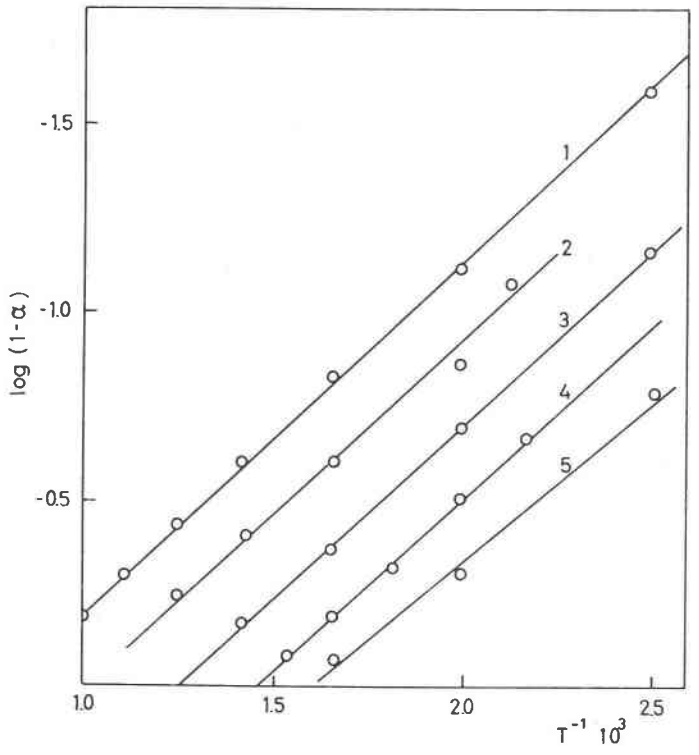

FIG. 11. log $(1-\alpha)$ against T^{-1}. 1, Muscovite. 2, Phlogopite I. 3, Biotite II (LF) 4, Biotite I (LF) 5, Phlogopite II.

From Fig. 11, it is seen that relation (13) is verified and an activation energy of 4.3 ± 0.1 kcal/proton gram is found for all the various micas studied. This observation appears to indicate that the activation energy of the delocalization process depends neither on the structure, nor on the chemical composition of the micas, nor on the direction of the OH bonds.

The factor B can be calculated from the intercept of the ordinate axis for $1/T=0$ (Fig. 11). We do not need the calculation to see that the delocalization parameter B is different for each mica. It may depend on the nature of the cations and on the population of the octahedral holes but it has a constant value for a given mica. As the chemical analyses are always partially uncertain, a large number of experiments would be necessary to determine the effect of the number and the nature of the cations. However, the comparison between the octahedral populations for three sites (Table 1) and the distribution of the corresponding B parameters in Fig. 11 shows that B is the highest for compositions which are the most divergent from the ideal di- and tri-octahedral structures.

This means that delocalization is more pronounced at low temperatures for intermediate di-trioctahedral compositions. The discussion in the appendix will develop this viewpoint.

It remains to consider the nature of the excited state of a delocalized proton.

A reasonable representation may be to depict the delocalized proton as jumping from one oxygen to another, passing through interstitial sites or vacancies. If the life time of a OH bond is smaller than 9×10^{-15} sec, which corresponds to an average fundamental frequency of 3660 cm^{-1}, the infrared radiation cannot detect its existence. Moreover, the 4.3 kcal activation energy may not be the height of the potential barrier, which

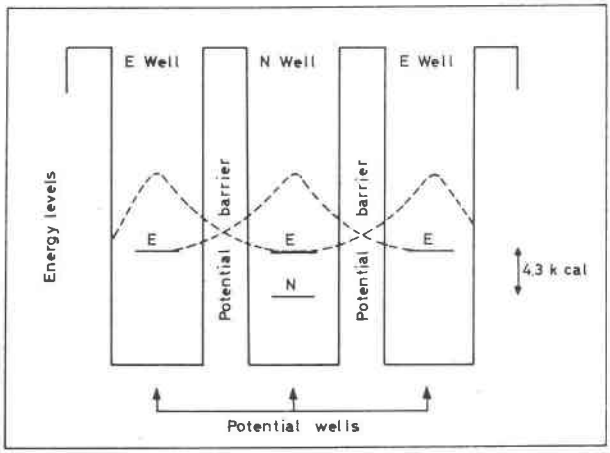

FIG. 12. Wave mechanical model proposed for the proton delocalization. N: potential well corresponding to the localized state. E: potential well involved in the delocalization process. Dashed line: schematic representation of the product of the conjugate proton wave functions with respect to the distance to the potential well centre.

would be much greater. If the model of a particle in a potential well is applied to the proton, it may be thought that the high potential barrier is passed over by a tunnelling effect. Suppose a proton at the E energy level (Fig. 12); it has a small probability of being in the domain of the potential barrier; during 9×10^{-15} sec, each proton may have the possibility to enter this domain at least once and may either proceed to the adjacent potential well or return to the initial one. In the first alternative, it has been delocalized. This representation would mean that the delocalization is continually effective and does not take account of the 4.3 kcal activation energy. It is then reasonable to suppose that the ground state of the proton in the potential well is not in E but in N (Fig. 12). For delocaliza-

tion, the proton has first to gain enough energy to achieve the E state, for example from various thermal effects and eventual slight modifications of the crystal field.

After the proton has left an N well, according to the suggested mechanism, the translation from E well to E well will occur until eventually a free N well is met by the moving particle. Translating protons do not contribute any more to the OH absorption band. The modification is, of course, reversible since cooling the sample strongly diminishes the probability of the N→E transition.

Appendix

As far as proton delocalization is studied below the dehydroxylation temperature, it may be considered as a reversible equilibrium process and it may be adequately represented by relationship (12):

$$K = \frac{c(1-\alpha)^2}{\alpha} \tag{12}$$

Again it must be emphasized that the functions $\alpha(T)$, represented in Fig. 8, cannot be extrapolated to $\alpha=0$ since K would then reach infinity at a finite temperature, which is impossible.

In terms of statistical thermodynamics, the equilibrium constant K may be written also as:

$$K = \frac{f_{H^+} f_{O^-}}{f_{OH} f_i^{Ni}} \tag{14}$$

where f_{H^+} is the partition function of H^+ in interstitial positions, f_{O^-} and f_{OH}, the partition functions of O^- and OH at lattice points respectively and f_i^{Ni} the partition functions of N_i interstitial sites accessible to the moving proton. f_{H^+} may be written as follows:

$$f_{H^+} = \frac{(2\pi mkT)^{3/2}}{h^3} \bar{V}_d g_{spin} e^{-W_i/kT} \tag{15}$$

The contribution of the translational kinetic energy of a proton to the partition function is equal to

$$\frac{(2\pi mkT)^{3/2}}{h^3} \bar{V}_d,$$

where m is the protonic mass and $\bar{V}_d$ the delocalization volume. g_{spin} is the nuclear spin weight and W_i the association energy of a proton with an interstitial site.

f_{OH} and f_{O^-} consist of the vibrational, electronic and zero point energy contributions or:

$$f_{OH} = \pi_i (1 - e^{-h\nu_i/kT})^{-1} g_{elec.(OH)} e^{E_{OH}/kT} \tag{16}$$

and

$$f_{O^-} = (1 - e^{-h\nu/kT})^{-1} g_{elec.(O^-)} e^{E_{O^-}/kT} \tag{17}$$

where E_{OH} and E_{O^-} are the energy of OH and O^- in the lattice points, ν_i and ν the fundamental vibration frequencies of OH and O^- respectively, $g_{elec.(OH)}$ and $g_{elec.(O^-)}$ the statistical weights of the corresponding lowest electronic states.

The partition function of the N_i interstitial sites actually involved in the delocalization of one proton is mainly composed from an energy contribution ($N_i E_i$):

$$f_i^{Ni} = e^{-N_i E_i/kT} \tag{18}$$

The vibrational terms in (16) and (17) being negligible because of the relatively high frequencies of the vibration bands, f_{O^-} and f_{OH} may be simplified. Therefore, from (18), (16) (17), (15) and (14) follows:

$$K = (2\pi mkT)^{3/2}h^{-3}\bar{V}_d g_{spin}\, g_{elec.(O^-)} g^{-1}_{elec.(OH)} e^{-\Delta E/kT} \tag{19}$$

where $\Delta E = W_i + E_{O^-} - E_{OH} - N_i E_i$. From (19) and (12) follows:

$$\log \frac{(1-\alpha)^2}{\alpha} - \frac{3}{2}\log T = \log A\bar{N}_i\bar{V}_d - \Delta E/2.303RT \tag{20}$$

where:

$$A = (2\pi mk)^{3/2}h^{-3} g_{spin}\, g_{elec.(O^-)} g^{-1}_{elec.(OH)}$$

It must be pointed out that in relation (12),c has been replaced by $\bar{N}_i^{-1}$, the number of interstitial sites to which *one* proton has access ($N_{OH^0} = 1$).

As shown in Fig. 13, the functions obtained by plotting

$$\left(\log \frac{(1-\alpha)^2}{\alpha} - \frac{3}{2}\log T\right)$$

against T^{-1} are linear. The parameters $\log A\bar{V}_d\bar{N}_i$ and ΔE are collected in Table 2: the thermal behaviors of micas are characterized by moderate variations of ΔE and by a

TABLE 2. ΔE (kcal/proton gram) AND $\log A\,\bar{V}_d\bar{N}_i$ OBTAINED FROM RELATIONSHIP (20)

Sample	E	$\log A\,\bar{V}_d\bar{N}_i$	θ	$<(1-\theta)\log(1-\theta)+\theta\log\theta$
Muscovite	7.6	−2.921	0.951	+0.0851
Phlogopite I	8.50	−2.612	0.028	+0.0551
Biotite II	9.3	−1.202	0.089	+0.130
Biotite I	10.3	−0.24	0.217	+0.227
Phlogopite II	10.4	+0.24	0.163	+0.200

change of $\bar{V}_d\bar{N}_i$ covering three orders of magnitude. From these results, $\bar{V}_d\bar{N}_i$ seems to be the lowest for samples in which the perfect di- or tri-octahedral compositions are approached and the highest for intermediate compositions. The same remark has been made previously for the B coefficient of the Boltzmann equation (13). This suggests that the delocalization process should involve octahedral free sites or vacancies. Each possible octahedral configuration builds a peculiar distribution of vacancies in the neighborhood of each OH ion and thus a peculiar delocalization volume. It may be assumed that the delocalization volume will be larger in octahedral layers characterized by a high number of statistical distributions of vacancies.

The number of distributions may be calculated easily from the octahedral population per three sites. In intermediate di- and tri-octahedral, the free sites fraction $0<\theta<1$, is defined as the unoccupied part among three octahedral sites and, per unit volume, the number of distributions of N free sites within $N_0 = \frac{1}{3}$ of the octahedral sites is $N_0!/N!(N_0-N)!$. It may be appropriate to suggest that the delocalization volume $\bar{V}d$ is proportional to the number of distributions, normalized for one proton, or:

$$\bar{V}_d = v_d \frac{\bar{N}_0!}{\bar{N}!(\bar{N}_0 - \bar{N})!}$$

The proportionality factor v_d may be considered as the average delocalization volume per distribution. From Stirling's approximation it follows:

$$\log \overline{V}_d = \log v_d - \overline{N}_0[(1-\theta)\log(1-\theta) + \theta \log \theta] \tag{21}$$

since $\theta = \overline{N}/\overline{N}_0$. Table 2 contains—$[(1-\theta)\log(1-\theta)+\theta \log \theta]$, calculated from the octahedral populations given in Table 1.

The characteristic properties of the distribution function—$[(1-\theta)\ln(1-\theta)+\theta \log \theta)]$ is to reach zero for $\theta=0$ and $\theta=1$ and to reach a maximum for $\theta=\frac{1}{2}$. This means that $\overline{V}_d$ should decrease to v_d for perfect dioctahedral and trioctahedral structures and to reach a maximum for $\theta=\frac{1}{2}$ i.e. for an hypothetical octahedral population of 2.5 cations per three sites. The thermal stability of this composition should be the lowest.

As shown in Table 2, the correlation predicted by (20) between $\log A\overline{V}_d\overline{N}_i$ and the distribution function of free octahedral sites is as good as it may be expected because of the relative uncertainty of chemical analyses.

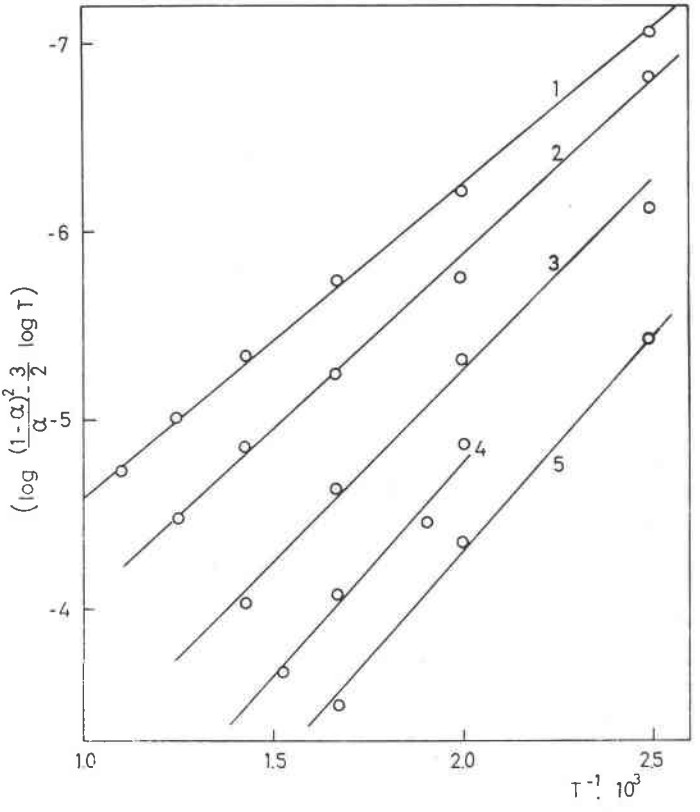

Fig. 13. $\left(\log \frac{(1-\alpha)^2}{\alpha} - \frac{3}{2}\log T\right)$ against T^{-1}. 1, Muscovite. 2, Phlogopite T. 3, Biotite II. 4, Biotite I. 5, Phlogopite II.

In conclusion, the main interest of this statistical thermodynamic treatment of the proton delocalization process is to show that perfect dioctahedral and trioctahedral lattices should have a higher thermal stability than intermediate compositions and this seems in agreement with the experimental results shown in Fig. 8.

Acknowledgments

The authors wish to thank Dr. G. W. Brindley of the Materials Research Laboratory, The Pennsylvania State University, for his interest in this study. The many valuable discussions with him during both the experimental work and preparation of this paper were especially appreciated.

Mica specimens were obtained by the courtesy of Professor L. Cahen, Director of the "Musée Royal d'Afrique Centrale" at Tervuren (Belgium), of Professor J. Moreau of this University and of Dr. G. W. Brindley, The Pennsylvania State University.

References

Eberhart, J. P. (1963) Étude de la transformation du mica muscovite par chauffage entre 700 et 1200° C. *Bull. Soc. Franc. Mineral. Crist.* **86,** 213–251.

Fripiat, J. J. and F. Toussaint (1963) Dehydroxylation of kaolinite. II Conductimetric measurements and infrared spectroscopy. *Jour. Phys. Chem.* **67,** 30–35.

Radoslovich, E. W. (1960) The structure of muscovite $KAl_2(Si_3Al)O_{10}(OH)_2$. *Acta Cryst.* **13,** 919–932.

Serratosa, J. M. and W. F. Bradley (1958a) Determination of the orientation of OH bond axis in layer silicates by infrared spectroscopy. *Jour. Phys. Chem.* **62,** 1164–1167.

——— (1958b) Infrared absorption of OH bonds in micas. *Nature* **181,** 111.

Smith, J. V. and H. S. Yoder (1956) Experimental and theoretical studies of the mica polymorphs. *Mineral Mag.* **31,** 209–235.

Tsuboi, M. (1950) On the position of the hydrogen atoms in the crystal structure of muscovite, as revealed by the infrared absorption. *Bull. Chem. Soc. Japan,* **23,** 83–88.

Vedder, W. (1964) Correlations between infrared spectrum and chemical composition of mica. *Am. Mineral.* **49,** 736–738.

——— and R. S. McDonald (1963) Vibration of the OH ions in the muscovite. *Jour. Chem. Phys.* **38,** 1583–1590.

Manuscript received, February 18, 1965; accepted for publication, July 13, 1965.